Article

Elevated NSD3 histone methylation activity drives squamous cell lung cancer

https://doi.org/10.1038/s41586-020-03170-y

Received: 30 April 2020

Accepted: 23 December 2020

Published online: 03 February 2021

Check for updates

Gang Yuan[1,13], Natasha M. Flores[2,13], Simone Hausmann[2], Shane M. Lofgren[2], Vladlena Kharchenko[3], Maria Angulo-Ibanez[4,5], Deepanwita Sengupta[1], Xiaoyin Lu[2], Iwona Czaban[3], Dulat Azhibek[3], Silvestre Vicent[6], Wolfgang Fischle[3], Mariusz Jaremko[3], Bingliang Fang[7], Ignacio I. Wistuba[8], Katrin F. Chua[4,5], Jack A. Roth[7], John D. Minna[9,10,11], Ning-Yi Shao[12]✉, Łukasz Jaremko[3]✉, Pawel K. Mazur[2]✉ & Or Gozani[1]✉

Amplification of chromosomal region 8p11–12 is a common genetic alteration that has been implicated in the aetiology of lung squamous cell carcinoma (LUSC)[1–3]. The *FGFR1* gene is the main candidate driver of tumorigenesis within this region[4]. However, clinical trials evaluating FGFR1 inhibition as a targeted therapy have been unsuccessful[5]. Here we identify the histone H3 lysine 36 (H3K36) methyltransferase NSD3, the gene for which is located in the 8p11–12 amplicon, as a key regulator of LUSC tumorigenesis. In contrast to other 8p11–12 candidate LUSC drivers, increased expression of *NSD3* correlated strongly with its gene amplification. Ablation of *NSD3*, but not of *FGFR1*, attenuated tumour growth and extended survival in a mouse model of LUSC. We identify an LUSC-associated variant NSD3(T1232A) that shows increased catalytic activity for dimethylation of H3K36 (H3K36me2) in vitro and in vivo. Structural dynamic analyses revealed that the T1232A substitution elicited localized mobility changes throughout the catalytic domain of NSD3 to relieve auto-inhibition and to increase accessibility of the H3 substrate. Expression of NSD3(T1232A) in vivo accelerated tumorigenesis and decreased overall survival in mouse models of LUSC. Pathological generation of H3K36me2 by NSD3(T1232A) reprograms the chromatin landscape to promote oncogenic gene expression signatures. Furthermore, NSD3, in a manner dependent on its catalytic activity, promoted transformation in human tracheobronchial cells and growth of xenografted human LUSC cell lines with amplification of 8p11–12. Depletion of NSD3 in patient-derived xenografts from primary LUSCs containing *NSD3* amplification or the NSD3(T1232A)-encoding variant attenuated neoplastic growth in mice. Finally, NSD3-regulated LUSC-derived xenografts were hypersensitive to bromodomain inhibition. Thus, our work identifies *NSD3* as a principal 8p11–12 amplicon-associated oncogenic driver in LUSC, and suggests that NSD3-dependency renders LUSC therapeutically vulnerable to bromodomain inhibition.

Many genes within the 8p11–12 amplicon could potentially contribute to oncogenesis (Extended Data Fig. 1a). However, the minimal region of amplification across many neoplasms with the 8p11–12 amplicon centres around *FGFR1* and the neighbouring gene and candidate oncogene *NSD3*[3,4,6,7]. Analysis of LUSC datasets from The Cancer Genome Atlas (TCGA) shows that *NSD3* and its immediate neighbours (for example, *FGFR1*) are the most commonly amplified 8p11–12 genes (Extended Data Fig. 1a). Overall, amplification of the genomic area spanning *NSD3* and *FGFR1* is one of the more common molecular alterations in LUSC (Extended Data Fig. 1b). Notably, for *NSD3*, gene amplification correlates strongly with increased mRNA expression; by contrast, there is little correlation between *FGFR1* gene copy number and mRNA expression[2,3] (Fig. 1a, Extended Data Fig. 1a, b). Accordingly, depletion of NSD3, but not depletion of FGFR1 or PLPP5 (encoded by the gene immediately adjacent to *NSD3*), in the 8p11–12-amplified ($8p11^{AMP}$) H520 LUSC cell line inhibited xenograft tumour growth (Fig. 1b, Extended Data Fig. 2a–e). These data point to NSD3, rather than FGFR1, as the mutational driver within the 8p11–12 amplicon in LUSC.

We established a robust mouse model of LUSC consisting of canonical LUSC alterations co-occurring with 8p11–12 amplification (constitutively active PI3K, overexpression of SOX2, and deletion of *CDKN2A* and *CDKN2B*, here named PSC mice; Extended Data Fig. 1b, Methods). PSC mice develop with high penetrance lung tumours characterized by LUSC-defining molecular hallmarks[8] (Extended Data Fig. 2f). In this model, increased NSD3 expression tracks with tumour progression, consistent with NSD3 overexpression being observed in about 60% of

A list of affiliations appears at the end of the paper.

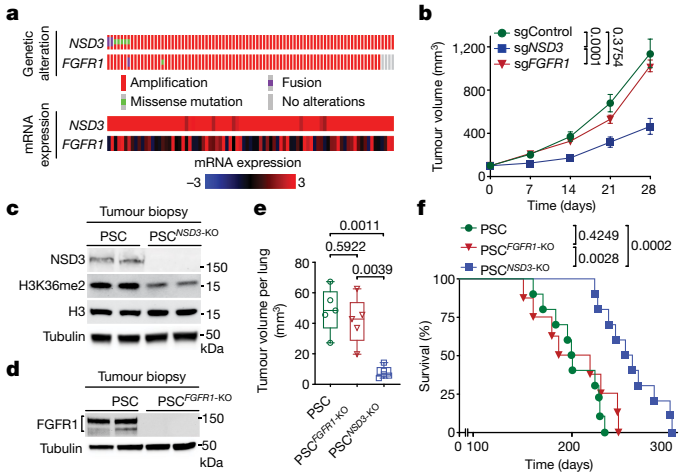

Fig. 1 | Deletion of *NSD3*, but not *FGFR1*, inhibits LUSC tumorigenesis in vivo. a, Analysis of 8p11–12-amplified LUSC datasets from TCGA indicates that increased mRNA expression (*Z*-score) of *NSD3*, but not *FGFR1*, correlates with gene amplification ($n = 85$ patients). **b**, Depletion of *NSD3*, but not *FGFR1*, attenuates xenograft growth of the 8p11^{AMP} LUSC cell line H520. Tumour volume quantification of H520 xenografts in immunocompromised mice ($n = 5$ mice for each group). **c**, **d**, Western blots of LUSC tumour lysates from PSC (control), PSC$^{NSD3\text{-}KO}$ (**c**) and PSC$^{FGFR1\text{-}KO}$ (**d**) mice with the indicated antibodies. Two independent and representative samples are shown for each genotype. Tubulin used as a loading control. **e**, Micro-computed tomography (μCT) analysis of tumour volume of the indicated mouse models ($n = 5$ mice for each group). Centre line, median; box limits, 75th and 25th percentiles; whiskers, minimum and maximum values. All data points are shown. *P* values determined by two-way analysis of variance (ANOVA) with Tukey's post hoc test (**b**, **e**). **f**, Kaplan–Meier survival curves of PSC ($n = 10$, median survival = 200.5 days), PSC$^{FGFR1\text{-}KO}$ ($n = 8$, median survival = 202.5 days) and PSC$^{NSD3\text{-}KO}$ ($n = 10$, median survival = 257 days) mice; *P* values determined by log-rank test.

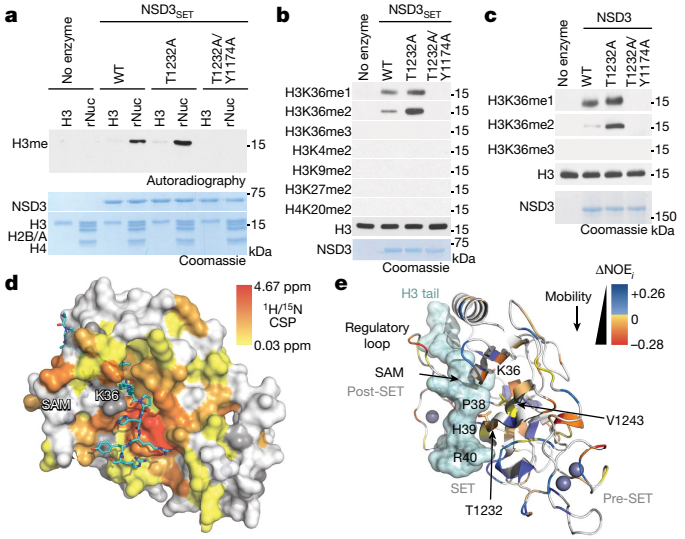

Fig. 2 | Molecular basis of increased H3K36me2 catalysis by NSD3(T1232A). a, In vitro methylation reactions of wild-type (WT) or mutant NSD3$_{SET}$ using recombinant free histone H3 or nucleosome (rNuc) and ^{3}H-SAM as substrates. No enzyme is a negative control. Top, autoradiography; bottom, Coomassie blue staining. **b**, Methylation assays on rNuc as in **a** with non-radiolabelled SAM. Western blots of reaction products shown with the indicated antibodies. H3 is shown as loading control. **c**, Methylation assays as in **b** with recombinant full-length wild-type or mutant NSD3. Data in **a**–**c** are representative of three or more biologically independent experiments with similar results. **d**, **e**, T1232A substitution induces widespread mobility changes in the NSD3 catalytic domain. **d**, Amide chemical shift perturbations between NSD3$_{SET\text{-}T1232A}$ and NSD3$_{SET}$ are mapped onto the surface representation of the NSD3$_{SET}$ structure (Protein Data Bank code (PDB) 6CEN) with docked H3.1 residues A29 to R42 (stick representation). Grey, prolines and residues missing amide assignments. **e**, Changes in heteronuclear {^{1}H}-^{15}N nuclear Overhauser effect (NOE) values plotted on the structure of NSD3 as in **d** in ribbon representation. T1232 and V1243 residues are indicated. Uncoloured residues, undetectable NOE changes. *i*, individual peaks.

LUSC samples (beyond the 20% that contain 8p11^{AMP}) and frequently co-occurring with PSC molecular alterations (Extended Data Fig. 2g–i).

Conditional *Fgfr1*$^{loxP/loxP}$ and *Nsd3*$^{loxP/loxP}$ mutant mice were generated. The mice were viable and fertile, and developed normally (Methods). In the PSC background, lung-specific deletion of *Nsd3* (PSC$^{NSD3\text{-}KO}$; Fig. 1c), but not *Fgfr1* (PSC$^{FGFR1\text{-}KO}$) (Fig. 1d), significantly attenuated tumour growth and cancer cell proliferation, while increasing apoptosis (Fig. 1e, Extended Data Fig. 2j–l). In survival studies, deletion of *Nsd3* extended the lifespan of PSC mice by about 30%, whereas *Fgfr1* knockout had no effect (Fig. 1f). Together, these data support a key in vivo role for NSD3 in LUSC tumorigenesis.

NSD3(T1232A) is a hyperactive variant

NSD3, NSD1, NSD2, and ASH1L are the four enzymes in mammals that specifically synthesize the euchromatin-associated H3K36me2 modification[9]. Depending on cell type, NSD1 and NSD2 are the main H3K36me2-generating enzymes, whereas the physiological context in which NSD3 regulates H3K36me2 is less clear[9]. Tumours lacking NSD3 showed lower global H3K36me2 than control tumours (Fig. 1c), suggesting an aetiological role for NSD3-catalysed H3K36me2 synthesis in *NSD3*-amplified LUSCs. We reasoned that we could test this idea in mice by transgenic expression of a hyperactive NSD3 variant, which would model the consequences of increased NSD3 catalysis resulting from elevated *NSD3* dosage on tumorigenesis. A recurrent hyperactivating NSD2 mutation is present in various cancers[9], suggesting that a functionally analogous cancer-associated mutation may be present in NSD3. We tested in vitro histone methylation activity for 35 TCGA-documented mutations within the NSD3 catalytic domain (Extended Data Fig. 3a–c). The variant with the highest activity was the T1232A substitution (NSD3(T1232A)), a recurrent cancer-associated mutation[10].

A recombinant NSD3 catalytic domain containing the T1232A substitution (NSD3$_{SET}$(T1232A)) shows stronger in vitro methylation activity on nucleosomes than does the wild-type domain (NSD3$_{SET}$), but this higher activity is abrogated when the substitution is paired with a catalytic mutant (NSD3$_{SET}$(T1232A/Y1174A)) (Fig. 2a, b, Extended Data Fig. 3d). Furthermore, NSD3$_{SET}$(T1232A) was more efficient than the wild-type enzyme in selectively generating H3K36me2 (Fig. 2b). Despite its higher activity, NSD3$_{SET}$(T1232A) behaved similarly to NSD3$_{SET}$ with respect to (i) nucleosomal versus free H3 substrate preference (Fig. 2a); (ii) methylation-state specificity, generating H3K36me1 or H3K36me2 but not H3K36me3 (Fig. 2b); and (iii) site-specific selectivity, methylating K36 but not several other histone lysine residues (Fig. 2b). Recombinant full-length NSD3(T1232A) behaved like the isolated catalytic domain in being hyperactive while retaining the same catalytic selectivity profile (Fig. 2c). Finally, overexpression of NSD3(T1232A), but not wild-type NSD3 or NSD3(T1232A/Y1174A), increased H3K36me2 levels in NSD2-depleted HT1080 fibrosarcoma cells (Extended Data Fig. 3e). These findings identify NSD3(T1232A) as a hyperactive cancer-associated mutant.

The enhanced activity of NSD3$_{SET}$(T1232A) versus NSD3$_{SET}$ was more evident in nucleosomes with longer linker DNA (187 versus 147 base pairs) (Extended Data Fig. 3f). The increase in catalysis, irrespective of linker DNA, was not mediated by the T1232A substitution significantly altering the binding affinity of NSD3 for nucleosomes or the cofactor methyl donor *S*-adenosyl-L-methionine (SAM) (Extended Data Fig. 4a,

Supplementary Table 1). High-resolution nuclear magnetic resonance (NMR) comparison of the protein backbones of $NSD3_{SET}$(T1232A) and $NSD3_{SET}$ in solution showed that the static structure is largely unaffected by the T1232A substitution (Extended Data Fig. 4b, c, Supplementary Table 1). By contrast, we found chemical shift perturbations of the backbone amide $^{1}H/^{15}N$ resonances, which serve as sensitive probes for local structural and allosteric effects, throughout the SET domain (Fig. 2d, Extended Data Fig. 4c, d). The highest chemical shift perturbations were centred around T1232A, with effects extending throughout the substrate-binding cleft and including the conserved NSD3 auto-regulatory loop[11,12] (Fig. 2d, Extended Data Fig. 4d, e). Consistent with these findings, backbone ^{15}N spin relaxation studies revealed multiple differences in local dynamics between $NSD3_{SET}$(T1232A) and $NSD3_{SET}$ concentrated at the substrate-binding cleft and auto-regulatory loop regions (Fig. 2e, Extended Data Fig. 4g, h, Supplementary Table 1). These data suggest that T1232A increases activity by enhancing the mobility of the auto-regulatory loop, which destabilizes the inhibitory state, acting together with the active site being rendered more accessible to the H3 substrate and direct, localized modification of the H3 binding surface. Indeed, the loss of the polar hydroxyl group in the T1232A mutant increases local hydrophobicity, which can alter H3 anchoring dynamics[13] (Fig. 2d, e). Introduction of a second alanine substitution at V1243, a residue adjacent to A1232 in the structure (T1232A/V1243A), is predicted to restore local surface hydrophobicity[13]. Accordingly, the methylation activity of a double alanine mutant ($NSD3_{SET}$(T1232A/V1243A)) was similar to that of the wild-type enzyme and lower than that of the single mutant $NSD3_{SET}$(T1232A), while $NSD3_{SET}$(V1243A) showed no activity and decreased thermal stability (Extended Data Fig. 4i, Supplementary Table 1). Thus, T1232A substitution induces changes in local dynamics at many residues within three key functional regions of the NSD3 catalytic domain that are likely to work together to increase catalysis of H3K36 methylation.

H3K36me2 deregulation accelerates LUSC

We used NSD3(T1232A) to model the consequences of elevated catalytic activity that would result from *NSD3* amplification for LUSC tumorigenesis in vivo. Mouse and human NSD3 are highly similar (94% overall; 98% in the catalytic domain), with mouse NSD3 (mNSD3) T1242 corresponding to human T1232 (Extended Data Fig. 5a). We generated Cre-inducible V5-tagged mNSD3(T1242A) mice and verified transgene expression in lung fibroblast cells transduced with Ad-Cre ex vivo (Extended Data Fig. 5b–e). In the PSC background, expression of mNSD3(T1242A) (here referred to as PSCN mice) accelerated tumour growth (Fig. 3a, b) and proliferation (Fig. 3c, d) while decreasing apoptosis (Extended Data Fig. 5f, g) relative to the control PSC group. For example, 90 days after Cre induction, when PSC mice have no detectable tumours, multiple growths were observed in the PSCN cohort (Fig. 3a). At 120 days, the tumour burden in PSCN mice was more than an order of magnitude greater than in control PSC mice (Fig. 3a, b). Consistent with these data, expression of mNSD3(T1242A) reduced lifespan in PSC mice by about 30% (Fig. 3e). In independent LUSC tumour biopsies, high NSD3 levels (due to mNSD3(T1242A) expression) resulted in markedly elevated H3K36me2 (Fig. 3f, Extended Data Fig. 5f). Moreover, mNSD3(T1242A)-driven tumours had higher levels of the oncoproteins MYC and BRD4 and phosphorylated 4EBP1 (a proxy for mTOR pathway activation) (Fig. 3f). Together, these data indicate that the activity of NSD3 substantially affects the clinical course and outcome of LUSC in vivo.

Comparison of cell lines derived from mNSD3(T1242A) and control PSC matched tumours (PSC_N and PSC_C, respectively) showed that H3K36me2 levels were higher in cells expressing mNSD3(T1242A), as was the case in tumours (Extended Data Fig. 5h). Furthermore, depletion of NSD3 in PSC_N cells resulted in a reduction in H3K36me2 levels (Fig. 3g). Transcriptomic data show that the effect of mNSD3(T1242A) expression status on the number of differentially expressed genes (DEGs) is, as expected, far greater when comparing PSCN to PSC tumour biopsies than for PSC_N cells with or without NSD3 depletion, in which NSD3 was depleted for a relatively short time before the analysis (Extended Data Fig. 5i, j, Supplementary Tables 2, 3). Nonetheless, the gene set enrichment analysis (GSEA) profiles of the tumour and cellular data sets show highly significant overlap with the same pathways, including strong correlations with MYC targets and mTOR signalling signatures (Fig. 3h, Extended Data Fig. 5k). Regulation of these genes (for example, *Prkaa2*, *Myc* and *Irgm1*) was observed in independent NSD3-depleted cell lines and depended on NSD3 catalytic activity (Extended Data Fig. 5l, m).

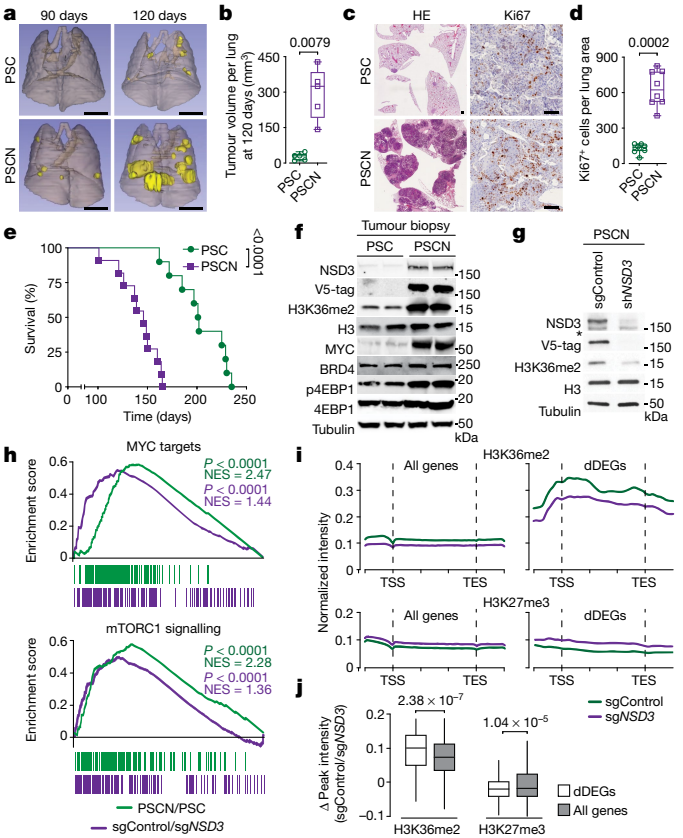

Fig. 3 | Mutant NSD3-mediated H3K36me2 synthesis promotes oncogenic programming and LUSC tumorigenesis. a, Representative μCT scans at 90 and 120 days after adenoviral Cre-mediated tumour induction in PSC and PSCN mice. Scale bars, 10 mm. **b**, Quantification of tumour volume as in **a** at 120 days ($n = 5$ mice for each group). **c**, Representative haematoxylin and eosin (HE) and immunohistochemical staining (Ki67) of lung tissue from PSCN and control PSC mutant mice ($n = 8$ mice for each group). Scale bars, 100 μm. **d**, Quantification of proliferation ($Ki67^+$ cells) as in **c**. *P* values determined by two-tailed unpaired *t*-test (**b**, **d**). **e**, Kaplan–Meier survival curves of PSCN ($n = 11$, median survival 145 days) and PSC (same data as in Fig. 1f, $n = 10$, median survival 200.5 days) mice; *P* value determined by log-rank test. **f**, Western blots of LUSC tumour lysates from PSCN and PSC mice with the indicated antibodies. Two independent and representative samples are shown for each genotype. **g**, Western blots of cell lysates from control (sgControl) or NSD3-depleted (sg*NSD3*) PSC_N cells with the indicated antibodies. H3 and tubulin shown as loading controls in **f**, **g**. **h**, GSEA identifies upregulation of hallmark gene sets (MYC targets and mTOR signalling (MSigDB: M5928, M5924)) in RNA sequencing (RNA-seq) data from PSCN versus PSC tumour biopsies and PSC_N cells with or without sg*NSD3* ($n = 3$ biologically independent samples per group). Normalized enrichment scores (NES) and nominal *P* values are provided (Methods). **i**, CUT&RUN profiles of H3K36me2 (top) and H3K27me3 (bottom) over averaged gene body for all genes or dDEGs in PSC_N cells with or without sg*NSD3*. **j**, Quantification of H3K36me2 and H3K27me3 peak intensity change in PSC_N cells with or without sg*NSD3* on the indicated gene sets. dDEGs $n = 234$, all genes $n = 16{,}091$. *P* values calculated by two-sided *t*-test.

Next, we used cleavage under targets and release using nuclease (CUT&RUN)[14] to profile the genomic distribution of H3K36me2 in PSC_N cells with or without NSD3 depletion. We also mapped H3K27me3, as the deposition of this important chromatin modification is directly antagonized by H3K36 methylation[9]. An averaged genome-wide distribution of H3K36me2 in PSC_N cells across all gene bodies showed that the signal peaks 5′ of the transcription start site (TSS), with a second smaller peak 3′ of the TSS, followed by a slow decay towards the 3′ end of a gene (Fig. 3i, Extended Data Fig. 6a). Upon NSD3 depletion, the intensity of the H3K36me2 signal is proportionally lower across the averaged gene unit, with little change in the overall pattern (Fig. 3i, Extended Data Fig. 6a). By contrast, the NSD3-dependent distribution of H3K36me2 specifically at the gene bodies of downregulated DEGs (dDEGs), the most likely direct targets of NSD3, diverged from the overall genome-wide pattern in two ways: (i) the baseline signal was 2–3-fold higher; and (ii) the signal distribution across the gene was distinct, with the most intense peak being 3′ rather than 5′ proximal to the TSS (Fig. 3i, Extended Data Fig. 6a). Furthermore, quantification of the difference between H3K36me2 peak signal intensities with or without NSD3 depletion revealed that the magnitude of peak change at dDEG bodies was significantly greater than the change observed genome-wide (Fig. 3j). Notably, relative to other genes, dDEGs showed both high H3K36me2 chromatin signal and high mRNA transcript levels (Extended Data Fig. 6b). These data suggest that robust transcription may predispose genes to NSD3 deregulation.

For H3K27me3, there was an overall increase in signal intensity upon NSD3 depletion genome-wide and at dDEGs, with no quantitative difference in the magnitude of change between the two gene groups (Fig. 3i, j). The inverse relationship between H3K36me2 and H3K27me3 in relation to NSD3 status extended to intergenic regions (Extended Data Fig. 6c, d). The pattern of diminished H3K36me2 and increased H3K27me3 upon NSD3 depletion was also observed at the level of individual dDEG tracks (Extended Data Fig. 6e). Finally, using chromatin immunoprecipitation (ChIP) assays, we observed a reduction in occupancy of mNSD3(T1242A) and H3K36me2 at target genes (*Prkaa2* and *Irgm1*) upon NSD3 depletion; this was reconstituted to control levels by complementation with catalytically active, but not catalytically dead, NSD3 (Extended Data Fig. 6f–h). Together, these data suggest that aberrant H3K36me2 synthesis by NSD3 directly regulates a LUSC-advancing gene expression program.

NSD3 promotes human LUSC tumorigenesis

To explore the role of NSD3 in human LUSC, we assembled the majority of publicly available human LUSC cell lines, including all five available $8p11^{AMP}$ cell lines, an $8p11^{AMP}$-negative NSD3-overexpressing cell line with a PSC-like genetic background, and six $8p11^{AMP}$-negative control cell lines lacking NSD3 overexpression, and used them to generate xenografts in mice (Fig. 4a, Extended Data Fig. 7a). Depletion of NSD3 impaired the formation of tumours from the $8p11^{AMP}$ or NSD3-overexpressing human LUSC cell lines but did not affect tumour growth from the six control cell lines (Fig. 4a, Extended Data Fig. 4b). The phenotype of the five $8p11^{AMP}$ LUSC-derived tumours is unlikely to result from non-specific DNA damage due to sgNSD3-targeted cutting within amplified regions[15], because: (i) sgRNA-mediated depletion of FGFR1 and PLPP5 had no effect on xenograft growth in $8p11^{AMP}$-positive H520 cells (Extended Data Fig. 2e); (ii) γH2AX levels were not altered by depletion of NSD3 in $8p11^{AMP}$ cell lines (Extended Data Figs. 2d, 7b); and (iii) depletion of NSD3 in the $8p11^{AMP}$ LUSC cell lines by RNA interference (RNAi) also attenuated xenograft growth (Fig. 4a, Extended Data Fig. 7c). Finally, complementing NSD3-depleted H520 cells with wild-type NSD3 or NSD3(T1232A) reconstituted xenograft tumour growth, whereas catalytically dead NSD3 or a short NSD3 isoform lacking the catalytic domain ($NSD3_{short}$) that has been previously implicated in breast cancer pathogenesis[6] both failed to reconstitute full xenograft growth (Fig. 4b, Extended Data Fig. 7d).

We next investigated the ability of NSD3 to cooperate with SOX2 to transform human tracheobronchial epithelial (AALE) cells[16]. As

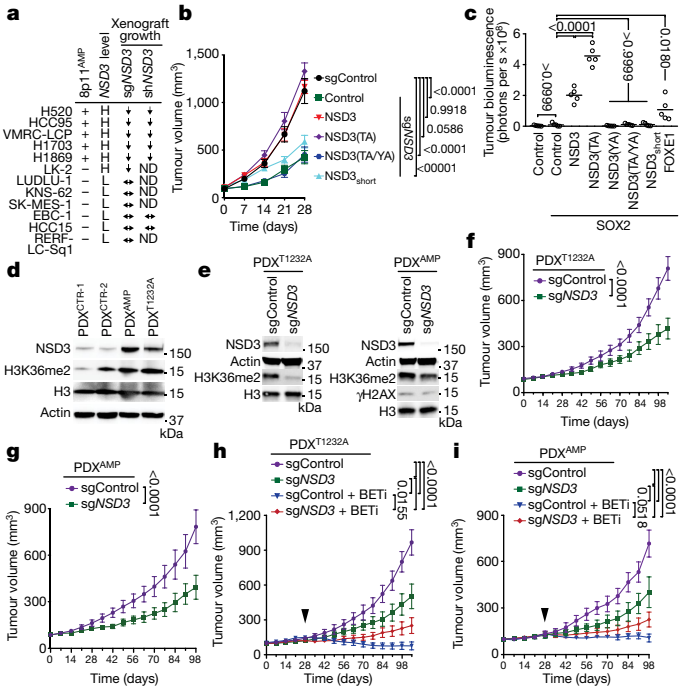

Fig. 4 | NSD3 promotes human lung cell transformation and xenograft tumour growth of LUSC cells and PDXs, and renders PDXs hypersensitive to BETi. a, NSD3 depletion attenuates xenograft tumour growth of $8p11^{AMP}$ and NSD3-overexpressing LUSC cell lines. Summary of xenograft tumour growth for the indicated cell lines treated with sg*NSD3* or a short hairpin RNA targeting *NSD3* (sh*NSD3*). *NSD3* levels: H, high mRNA (*Z*-score > 1.0); L, low mRNA (*Z*-score < 1.0). Scoring was consistent with relative protein levels (Extended Data Fig. 7a, b). Xenograft tumour growth: ↓, reduced; ↔, no change (Extended Data Fig. 7b, c); ND, not determined. **b**, NSD3 catalytic activity is required for full H520 xenograft tumour growth. Tumour volume change of H520 xenografts reconstituted with the indicated V5-tagged CRISPR-resistant NSD3 derivatives in immunocompromised mice ($n = 5$ mice, for each group).TA, T1232A; YA, Y1174A. **c**, NSD3 and NSD3(T1232A) transform SOX2-expressing AALE cells in vivo. Quantification of tumour size determined by bioluminescence of AALE cells grafted under the renal capsule and expressing the indicated plasmids plus the AkaLuc reporter ($n = 5$ mice for each group; Methods). FOXE1 is a positive control; NSD3 and NSD3(T1232A) versus FOXE1, $P < 0.0001$. Horizontal lines denote median. **d**, Western blots of lysates from the indicated LUSC PDX samples and using the indicated antibodies. H3 and actin are loading controls. **e**, Western blots as in **d** of lysates from PDX^{T1232A} and PDX^{AMP} cells with or without sg*NSD3* treatment. **f**, **g**, PDX tumour volumes of PDX^{T1232A} (**f**) and PDX^{AMP} tumours (**g**) with or without sg*NSD3* in immunocompromised mice ($n = 5$ for each group). **h**, **i**, Tumour volumes of PDX^{T1232A} (**h**) and PDX^{AMP} tumours (**i**) with or without sgNSD3 and with or without BETi (AZD5153; 2.5 mg kg^{-1}, intraperitoneal) treatments as indicated ($n = 5$ mice for each group). Control mice received vehicle (placebo) treatment. Arrowhead indicates start of the treatment. *P* values determined by two-way ANOVA with Tukey's post hoc test (**b**, **c**, **h**, **i**) or two-tailed unpaired *t*-test. (**f**, **g**). Data are represented as mean ± s.e.m. (**b**, **f**–**i**).

previously reported, ectopic expression of SOX2 with a second transcription factor (FOXE1) promotes anchorage-independent growth of AALE cells[16]. We found that ectopic expression of SOX2 with either wild-type NSD3 or NSD3(T1232A) was more efficient in transforming AALE cells than SOX2 with FOXE1, with SOX2– NSD3(T1232A) showing the greatest promotion of anchorage-independent growth in vitro (Extended Data Fig. 7e–g) and tumour growth in vivo (Fig. 4c, Extended Data Fig. 7e, h). By contrast, catalytically dead NSD3 and $NSD3_{short}$ did not promote AALE transformation (Fig. 4c, Extended Data Fig. 7e–h). Together, these data suggest that NSD3, via its catalytic activity, promotes tumour growth of human LUSC cells and oncogenic transformation of human AALE cells.

To further investigate the roles of the NSD3–H3K36me2 axis in human cancer, we screened a collection of 37 LUSC patient-derived xenograft (PDX) samples for NSD3 alterations. Of these, one contained NSD3(T1232A) (PDX^{T1232A}), twelve had amplification of *NSD3* (PDX^{AMP}), and the others had no NSD3 alteration (PDX^{CTR}) (Extended Data Fig. 8 and data not shown). We selected four PDXs (PDX^{T1232A}, $PDX^{AMP\text{-}1}$ and two PDX^{CTR}s), which apart from the NSD3 alterations had similar mutational profiles (for example, PSC signature), for further analysis. In comparison to PDX^{CTR} samples, NSD3 levels were higher in PDX^{T1232A} cells and highest in $PDX^{AMP\text{-}1}$ cells (Fig. 4d). H3K36me2 levels in the PDX^{T1232A} and $PDX^{AMP\text{-}1}$ cells were comparable to one another and elevated relative to controls (Fig. 4d); this pattern of similar H3K36me2 abundance in PDX^{T1232A} and $PDX^{AMP\text{-}1}$ cells, while the former has lower NSD3 levels, is consistent with hyperactivity of NSD3(T1232A). NSD3 depletion, which resulted in loss of H3K36me2, attenuated the growth of PDX^{T1232A} and $PDX^{AMP\text{-}1}$ xenograft tumours (Fig. 4e–g) but did not affect the growth of PDX^{CTR} samples (Extended Data Fig. 9a, b). NSD3 depletion also inhibited the growth of an independent $8p11^{AMP}$ PDX sample (Extended Data Fig. 9c). Thus, a subset of PDXs from primary LUSC human tumours are NSD3-regulated and selectively sensitive to NSD3 depletion.

NSD3 sensitizes LUSC to bromodomain inhibition

Although at present there is no NSD3 catalytic inhibitor that can be used in a physiological setting, we speculated that selection for NSD3-dependency may confer adaptive vulnerability of LUSC to drugs that target known cancer pathways. To test this idea, we screened a library comprising 285 characterized inhibitors covering about 170 cancer targets to identify drugs that are more effective in PSC_N than in PSC_C cells. The four bromodomain inhibitors (BETi) in the library exhibited the highest differential lethality, consistent with BRD4 interacting directly with NSD3 in LUSC cells[17,18] (Supplementary Table 4, Extended Data Fig. 9d). Under normal conditions, PSC_N cells proliferate more rapidly than PSC_C cells (Extended Data Fig. 9e). However, treatment with the BETi AZD5153[19], which has a modest effect on PSC_C cell proliferation, inhibited the expression of NSD3 target genes and the proliferation of PSC_N cells (Extended Data Fig. 9e, f). NSD3-dependent BETi sensitivity was also observed in PDXs; active growth of PDX^{T1232A} and PDX^{AMP} tumours stalled in response to BETi treatment, a phenotype that was weakened by NSD3 depletion (Fig. 4h, i). By contrast, PDX^{CTR} samples were moderately responsive to BETi therapy independent of NSD3 (Extended Data Fig. 9g, h). Thus, the oncogenic advantage provided by NSD3 to LUSC potentially comes with a cost—hypersensitivity to BETi—that represents a clinically actionable vulnerability.

Summary

LUSC, one of the leading causes of cancer-related mortality worldwide, is characterized by several well-defined driver mutations. However, in contrast to malignancies such as lung adenocarcinoma, in which targeted therapy approaches have been encouraging, translating similar strategies for LUSC has been difficult. Our results show that NSD3 has a key role in LUSC—a finding with potential prognostic and therapeutic relevance for the estimated 100,000 patients diagnosed worldwide each year with $8p11^{AMP}$ LUSC[20]. We propose a model in which NSD3, via H3K36me2, acts as an epigenetic deregulator to facilitate the expression of oncogenesis-promoting genes (Extended Data Fig. 10). The genes that are most affected by NSD3 depletion tend to be marked by high basal H3K36me2 and are robustly transcribed. These features are consistent with the vulnerability of NSD3-regulated LUSC to BETi, as this drug class targets active transcription[21]. Indeed, NSD3 depletion was recently identified as a strong sensitizer of acute myeloid leukaemia cells to BETi[22]. Thus, while clinical NSD3 inhibitors are presently unavailable, the increased sensitivity of NSD3-regulated LUSC to BETi may expand the narrow therapeutic window for these medicines[21]. Finally, the oncogenic activity of NSD3 is likely to extend beyond LUSC, as the 8p11–12 amplicon is a common molecular signature of breast cancer and other malignancies[7].

Online content

Any methods, additional references, Nature Research reporting summaries, source data, extended data, supplementary information, acknowledgements, peer review information; details of author contributions and competing interests; and statements of data and code availability are available at https://doi.org/10.1038/s41586-020-03170-y.

1. Balsara, B. R. et al. Comparative genomic hybridization analysis detects frequent, often high-level, overrepresentation of DNA sequences at 3q, 5p, 7p, and 8q in human non-small cell lung carcinomas. *Cancer Res.* **57**, 2116–2120 (1997).
2. Tonon, G. et al. High-resolution genomic profiles of human lung cancer. *Proc. Natl Acad. Sci. USA* **102**, 9625–9630 (2005).
3. Rooney, C. et al. Characterization of FGFR1 locus in sqNSCLC reveals a broad and heterogeneous amplicon. *PLoS ONE* **11**, e0149628 (2016).
4. Weiss, J. et al. Frequent and focal FGFR1 amplification associates with therapeutically tractable FGFR1 dependency in squamous cell lung cancer. *Sci. Transl. Med.* **2**, 62ra93 (2010).
5. Lim, S. H. et al. Efficacy and safety of dovitinib in pretreated patients with advanced squamous non-small cell lung cancer with FGFR1 amplification: a single-arm, phase 2 study. *Cancer* **122**, 3024–3031 (2016).
6. Yang, Z. Q., Liu, G., Bollig-Fischer, A., Giroux, C. N. & Ethier, S. P. Transforming properties of 8p11-12 amplified genes in human breast cancer. *Cancer Res.* **70**, 8487–8497 (2010).
7. Turner-Ivey, B. et al. Development of mammary hyperplasia, dysplasia, and invasive ductal carcinoma in transgenic mice expressing the 8p11 amplicon oncogene NSD3. *Breast Cancer Res. Treat.* **164**, 349–358 (2017).
8. Travis, W. D. Lung cancer pathology: current concepts. *Clin. Chest Med.* **41**, 67–85 (2020).
9. Husmann, D. & Gozani, O. Histone lysine methyltransferases in biology and disease. *Nat. Struct. Mol. Biol.* **26**, 880–889 (2019).
10. Landau, D. A. et al. Evolution and impact of subclonal mutations in chronic lymphocytic leukemia. *Cell* **152**, 714–726 (2013).
11. Qiao, Q. et al. The structure of NSD1 reveals an autoregulatory mechanism underlying histone H3K36 methylation. *J. Biol. Chem.* **286**, 8361–8368 (2011).
12. Graham, S. E., Tweedy, S. E. & Carlson, H. A. Dynamic behavior of the post-SET loop region of NSD1: implications for histone binding and drug development. *Protein Sci.* **25**, 1021–1029 (2016).
13. Yang, S. et al. Molecular basis for oncohistone H3 recognition by SETD2 methyltransferase. *Genes Dev.* **30**, 1611–1616 (2016).
14. Skene, P. J. & Henikoff, S. An efficient targeted nuclease strategy for high-resolution mapping of DNA binding sites. *eLife* **6**, e21856 (2017).
15. Munoz, D. M. et al. CRISPR screens provide a comprehensive assessment of cancer vulnerabilities but generate false-positive hits for highly amplified genomic regions. *Cancer Discov.* **6**, 900–913 (2016).
16. Bass, A. J. et al. *SOX2* is an amplified lineage-survival oncogene in lung and esophageal squamous cell carcinomas. *Nat. Genet.* **41**, 1238–1242 (2009).
17. Zhang, Q. et al. Structural mechanism of transcriptional regulator NSD3 recognition by the ET domain of BRD4. *Structure* **24**, 1201–1208 (2016).
18. Shen, C. et al. NSD3-short is an adaptor protein that couples BRD4 to the CHD8 chromatin remodeler. *Mol. Cell* **60**, 847–859 (2015).
19. Bradbury, R. H. et al. Optimization of a series of bivalent triazolopyridazine based bromodomain and extraterminal inhibitors: the discovery of (3R)-4-[2-[4-[1-(3-methoxy-[1,2,4]triazolo[4,3-b]pyridazin-6-yl)-4-piperidyl]phenoxy]ethyl]-1,3-dimethyl-piperazin-2-one (AZD5153). *J. Med. Chem.* **59**, 7801–7817 (2016).
20. Siegel, R. L., Miller, K. D. & Jemal, A. Cancer statistics, 2019. *CA Cancer J. Clin.* **69**, 7–34 (2019).
21. Cochran, A. G., Conery, A. R. & Sims, R. J. III. Bromodomains: a new target class for drug development. *Nat. Rev. Drug Discov.* **18**, 609–628 (2019).
22. Lin, K. H. et al. Using antagonistic pleiotropy to design a chemotherapy-induced evolutionary trap to target drug resistance in cancer. *Nat. Genet.* **52**, 408–417 (2020).

[1]Department of Biology, Stanford University, Stanford, CA, USA. [2]Department of Experimental Radiation Oncology, The University of Texas MD Anderson Cancer Center, Houston, TX, USA. [3]Division of Biological and Environmental Science and Engineering, King Abdullah University of Science and Technology, Thuwal, Saudi Arabia. [4]Department of Medicine, Stanford University School of Medicine, Stanford, CA, USA. [5]Geriatric Research, Education, and Clinical Center, Veterans Affairs Palo Alto Health Care System, Palo Alto, CA, USA. [6]University of Navarra, Center for Applied Medical Research, Pamplona, Spain. [7]Department of Thoracic and Cardiovascular Surgery, The University of Texas MD Anderson Cancer Center, Houston, TX, USA. [8]Department of Translational Molecular Pathology, The University of Texas MD Anderson Cancer Center, Houston, TX, USA. [9]Hamon Center for Therapeutic Oncology Research, University of Texas Southwestern Medical Center, Dallas, TX, USA. [10]Department of Internal Medicine, University of Texas Southwestern Medical Center, Dallas, TX, USA. [11]Department of Pharmacology, University of Texas Southwestern Medical Center, Dallas, TX, USA. [12]Faculty of Health Sciences, University of Macau, Macau SAR, China. [13]These authors contributed equally: Gang Yuan, Natasha M. Flores. ✉e-mail: nshao@um.edu.mo; lukasz.jaremko@kaust.edu.sa; pkmazur@mdanderson.org; ogozani@stanford.edu